Published in final edited form as:
Clin Cancer Res. 2015 January 15; 21(2): 386–395. doi:10.1158/1078-0432.CCR-14-0964.

Metabolic Imaging of Pancreatic Ductal Adenocarcinoma Detects Altered Choline Metabolism

Marie-France Penet[1,2,*], **Tariq Shah**[1,*], **Santosh Bharti**[1], **Balaji Krishnamachary**[1], **Dmitri Artemov**[1,2], **Yelena Mironchik**[1], **Flonné Wildes**[1], **Anirban Maitra**[2,3], and **Zaver M. Bhujwalla**[1,2,#]

[1]JHU ICMIC Program, Division of Cancer Imaging Research, The Russell H. Morgan Department of Radiology and Radiological Science, The Johns Hopkins University School of Medicine, Baltimore MD

[2]Sidney Kimmel Comprehensive Cancer Center, The Johns Hopkins University School of Medicine, Baltimore MD

[3]Departments of Pathology and Translational Molecular Pathology, UT MD Anderson Cancer Center, Houston TX

Abstract

Purpose—Pancreatic ductal adenocarcinoma (PDAC) is an aggressive and lethal disease that develops relatively symptom-free and is therefore advanced at the time of diagnosis. The absence of early symptoms and effective treatments has created a critical need for identifying and developing new noninvasive biomarkers and therapeutic targets.

Experimental Design—We investigated the metabolism of a panel of PDAC cell lines in culture and noninvasively *in vivo* with ^{1}H magnetic resonance spectroscopic imaging (MRSI) to identify noninvasive biomarkers and uncover potential metabolic targets.

Results—We observed elevated choline-containing compounds in the PDAC cell lines and tumors. These elevated choline-containing compounds were easily detected by increased total choline (tCho) *in vivo*, in spectroscopic images obtained from tumors. Principal component analysis of the spectral data identified additional differences in metabolites between HPNE and neoplastic PDAC cells. Molecular characterization revealed overexpression of choline kinase (Chk)-α, choline transporter 1 (CHT1), and choline transporter-like protein 1 (CTL1) in the PDAC cell lines and tumors.

Conclusions—Collectively, these data identify new metabolic characteristics of PDAC and reveal potential metabolic targets. Total choline detected with ^{1}H MRSI may provide an intrinsic, imaging-probe independent biomarker to complement existing techniques in detecting PDAC. The expression of Chk-α, CHT1, and CTL1 may provide additional molecular markers in aspirated cytological samples.

[#]Correspondence to: Zaver M. Bhujwalla, Ph.D., Department of Radiology, Johns Hopkins University School of Medicine, 208C Traylor Building, 720 Rutland Avenue, Baltimore, MD 21205, USA. Phone: 410-955-9698, Fax: 410-614-1948, zaver@mri.jhu.edu.
[*]These authors contributed equally

No conflicts of interest to disclose

Keywords

pancreatic ductal adenocarcinoma; choline phospholipids; metabolism; noninvasive detection; targets

Introduction

Pancreatic cancer is the fourth leading cause of cancer death in the USA and leads to approximately 227,000 deaths per year worldwide (1). Early-stage pancreatic cancer is clinically silent, and most patients presenting with symptoms attributable to pancreatic cancer have advanced disease. These symptoms become apparent after the tumor invades surrounding tissues or metastasizes to distant organs, resulting in abdominal or mid-back pain, obstructive jaundice, and weight loss (1). Most pancreatic cancers are histologically classified as pancreatic ductal adenocarcinoma (PDAC) (2), and have a 5 year survival rate of only 6% (3). The poor prognosis of PDAC arises from a combination of late-stage diagnosis and limited response to chemotherapy and radiotherapy, both of which are partly due to the strong desmoplastic stroma that limits delivery of diagnostic imaging probes and therapeutic agents (4). Similarities in the clinical behavior and imaging features of PDAC and chronic pancreatitis further complicate the detection of PDAC (5). The unavailability of targeted agents for this disease has also significantly impeded effective treatment.

Although inroads are being made in developing molecular imaging probes such as plectin-1 targeted peptides to detect PDAC (6), these have not been clinically translated. There is an urgent need for noninvasive clinically translatable biomarkers of PDAC. Magnetic resonance spectroscopy (MRS) is being evaluated in the diagnosis of several solid malignancies such as brain, prostate and breast cancer (7). An elevation of total choline (tCho) is a metabolic hallmark in the spectra of cancers imaged with ^{1}H MRS (7). tCho, observed as a single peak *in vivo*, consists of three choline-containing metabolites, which can be resolved through high-resolution proton spectroscopy into phosphocholine (PC), glycerophosphocholine (GPC) and free choline (Cho). Increased PC in tumors is the primary cause of the elevated tCho and is due to an overexpression of the choline kinase (*Chk*)-α gene as well as increased expression of choline transporters (8–10). Chk catalyzes the phosphorylation of Cho using ATP, as a phosphate donor, to produce PC. An elevation of choline uptake by choline transporters, followed by phosphorylation by choline kinase can also increase endogenous PC (11). Increased expression of the high-affinity choline transporter CHT1 with a K_m of ~ 2 μM, also called solute carrier family 5 member 7 (SLC5A7) (12), has been previously observed in breast cancer cells (10). Another choline transporter, choline transporter-like protein 1 (CTL1) with a K_m of ~ 68 μM, was found to be overexpressed in human lung and colon carcinoma cells (13, 14).

Here, we have characterized the metabolic profile, especially choline phospholipid metabolism, in a panel of PDAC cell lines, and tumor xenografts derived from these PDAC cells, implanted subcutaneously or orthotopically in the pancreas, using ^{1}H magnetic resonance spectroscopic imaging (MRSI) and MRS. Significantly elevated PC and tCho were observed in the PDAC cell lines, compared to an immortalized non-neoplastic

pancreatic cell line. Increases in PC and tCho observed in PDAC cells were paralleled in tumors derived from the PDAC cells, with elevated tCho observed in metabolic images from *in vivo* tumors. Molecular characterization of these cells and tumors identified overexpression of Chk-α, CHT1 and CTL1 as the primary causes of increased tCho and PC. These data identify tCho as a potential intrinsic biomarker to detect PDAC noninvasively with ^{1}H MR spectroscopic metabolic imaging. Enzymes in choline phospholipid metabolism pathway, such as Chk-α, may provide potential therapeutic targets for PDAC treatment.

Methods

Cell lines and tumor implantation

Eight PDAC cell lines and one immortalized pancreatic cell line were used in the study. Details about the cell lines are provided in Table 1. BxPC3 and Panc1 were obtained from ATCC (American Tissue Culture Collection, Manassas, VA). Pa02C, Pa03C, Pa04C, Pa09C, Pa20C and Pa28C have been previously described (15). Pa02C and Pa03C were derived from liver metastases, Pa04C from lung metastasis, and BxPC-3, Panc-1, Pa09C, Pa20C, and Pa28C were derived from primary adenocarcinomas. For comparison, we used human pancreatic nestin expressing (HPNE) cells from ATCC. HPNE cells were derived from non-neoplastic human pancreas that stably express human telomerase reverse transcriptase (hTERT) after transduction with a retroviral expression vector containing the hTERT gene. Panc1, BxPC3, Pa03C, Pa04C, Pa20C and Pa28C cells were cultured in DMEM (Sigma, St. Louis, MO) with 10% fetal bovine serum (FBS), 100 units/ml penicillin, 100 μg/ml streptomycin, 25 mM glucose and 4 mM glutamine. Pa02C and Pa09C were cultured in RPMI-1640 (Sigma) with 20% FBS, 100 units/ml penicillin, 100 μg/ml streptomycin, 12.5 mM glucose and 2 mM glutamine. hTERT-HPNE cells were cultured according to the protocol recommended by ATCC. The base medium was a combination of 75% DMEM without glucose (Sigma), with additional 2 mM glutamine, 1.5 g/L sodium bicarbonate and 25% M3 Base medium (Incell Corp., San Antonio, TX). To make complete growth medium, 5 % FBS, 10 ng/ml human recombinant epidermal growth factor, 5.5 mM glucose, and 750 ng/ml puromycin were added to the base medium. DMEM and RPMI have comparable concentrations of choline chloride (~ 0.021– 0.028 mM).

Cells were cultured in standard cell culture incubator conditions at 37° C in a humidified atmosphere containing 5% CO_2. Subcutaneous tumors were generated by inoculating 2×10^6 cells suspended in 0.05 ml of Hanks balanced salt solution in the flank of severe combined immunodeficient (SCID) male mice. Orthotopic implantation was performed as previously described (16). Viable tumor pieces of ~1 mm^3 harvested from subcutaneous tumors were implanted into the pancreas of anesthetized male SCID mice *via* a subcostal left incision of ~1 cm. All surgical procedures and animal handling were performed in accordance with protocols approved by the Johns Hopkins University Institutional Animal Care and Use Committee, and conformed to the Guide for the Care and Use of Laboratory Animals published by the NIH.

In vivo MRSI

Anesthetized tumor bearing mice were imaged at 4.7T for subcutaneous tumors or at 9.4T for orthotopic tumors using Bruker Biospec MR scanners (Bruker Biospin Corp., Billerica, MA). Body temperature of the animals was maintained in the magnet by a thermostat-regulated heating pad. Localized ^{1}H MR spectra were acquired using a 15 mm diameter home-built solenoid coil placed around the subcutaneous tumor or a 30 mm Bruker (Bruker Biospin Corp.) volume coil placed around the torso of the orthotopic tumor bearing mice. Spectra from a 4 mm thick central slice localized within the tumor were acquired with a 16 mm field of view (FOV) for subcutaneous tumors, or 32 mm FOV for orthotopic tumors, and zero-filled to an in-plane spatial resolution of 1 mm × 1 mm. Spectra were acquired with 8 scans per phase encode step, an echo time (TE) of 272 ms for subcutaneous tumors, and 135 ms for orthotopic tumors, and a repetition time (TR) of 1059 ms for subcutaneous tumors, and 1500 ms for orthotopic tumors, using a 2D-CSI (chemical shift imaging) sequence with VAPOR (VAriable Pulse power and Optimized Relaxation delays) water suppression (17). These acquisition parameters were optimized to obtain a good tCho signal from the tumors in less than 35 minutes. Reference 2D-CSI images of the unsuppressed water signal were acquired from the tumors with a TE of 20 ms, a TR of 1059 ms, and 2 scans per phase encode step, with all other parameters remaining the same. Quantitative maps of tCho were generated from the spectroscopic images using unsuppressed water signal as an internal reference (18). Quantitative metabolic maps were generated using in-house IDL programs. For orthotopic tumors, single voxel PRESS ^{1}H spectra were also acquired with a TE of 67.5 ms, a TR of 1500 ms, and voxel size of 5 × 5 × 5 mm^{3}.

MR spectroscopy of dual phase extracts

Cell and tumor extracts were obtained using a dual-phase extraction method with methanol/chloroform/water (1/1/1) (19). Briefly, approximately 1.5 × 10^{7} cells were harvested by trypsinization, washed twice with saline, and pooled into a glass centrifuge tube. Cell pellets were suspended in ice-cold methanol, vigorously vortexed, and kept on ice for 10 minutes. Next, 4 ml of chloroform and 4 ml of ice-cold water were added, and the solution was vortexed. To obtain tumor extracts, tumors were freeze-clamped and ground to powder. Ice-cold methanol was added, and the tumor extract samples were homogenized. Chloroform and ice-cold water were finally added. Cell and tumor extract samples were kept at 4°C overnight for phase separation. Samples were then centrifuged for 30 minutes at 15,000 g at 4°C to separate the phases. The water/methanol phase containing the water-soluble metabolites was treated with chelex (Sigma) for 10 minutes on ice to remove divalent cations. The chelex beads were removed through filtration. Methanol was then removed by rotary evaporation, and the remaining water phase was lyophilized and stored at −20°C. Water-soluble samples were dissolved in 0.5 ml of D_2O (Sigma) containing 3-(trimethylsilyl) propionic-2,2,3,3,-d4 acid (TSP) (Sigma) as an internal concentration standard (sample pH of 7.4). Fully relaxed ^{1}H MR spectra of the extracts were acquired on a Bruker Avance 500 spectrometer operating at 11.7 T (Bruker BioSpin Corp., Billerica, MA) using a 5-mm HX inverse probe, and the following acquisition parameters: 30° flip angle, 6000 Hz sweep width, 9.5 s repetition time, time-domain data points of 32K, and 128 transients (19). Spectra were analyzed using Bruker TOPSPIN 2.1 software (Bruker BioSpin). Integrals of the metabolites of interest were determined and normalized to the

number of cells and to the tumor weight, respectively. To determine concentrations, metabolite peak integration values from ^{1}H spectra were compared to the internal standard. Metabolites were estimated from at least three experimental samples from each cell line to obtain averaged values. Statistical significance was evaluated using the Student t-test. *P*-values ≤ 0.05 were considered statistically significant unless otherwise stated.

Principal component analysis (PCA) of MR spectral data

Single pulse MR spectra obtained from pancreatic cell lines were subjected to multivariate PCA. Raw spectral data were processed using TOPSPIN 2.1, and regions between 0.5 and 9.0 ppm were exported as raw data points using Bruker AMIX software (Version 3.8.7) (20). The resulting data matrices with normalized integral values were exported into Microsoft Office Excel 2010. The region from 4.5–5.2 ppm was excluded from the analysis to remove the residual signal of HOD and water. The data obtained were normalized by dividing each integral of the segment by the total area of the spectrum to compensate for differences in overall metabolite concentration between individual samples that can arise due to dilution errors. The whole matrix was imported into Matlab environments (MATLAB R2012b, 8.0.0.783, The MathWorks, Inc.) for spectral alignments. Icoshift algorithm for spectral alignments was used to remove the small chemical shift drifts in the spectra arising because of pH/ionic variations (20). The matrix was further imported to 'The Unscrambler X' Software package (Version 10.0.1, CAMO Software Inc.) for PCA.

Immunoblot of cells and tumors extracts

Proteins were extracted from cells, from freeze-clamped subcutaneous or orthotopic tumors, and from normal mouse pancreas, using radioimmunoprecipitation assay (RIPA) lysis buffer fortified with a protease inhibitor cocktail, dithiothreitol, phenylmethylsulfonyl fluoride, sodium orthovanadate, and sodium fluoride (Sigma). Protein lysate from a normal human pancreas was obtained from OriGene (OriGene, Rockville, MD). Protein concentration was estimated using the Bradford Bio-Rad protein assay kit (Bio-Rad, Hercules, CA). Approximately 60 – 75 μg of total protein were resolved on 10% SDS-PAGE, transferred onto nitrocellulose membranes, and probed for 2 h at room temperature with an in-house human specific rabbit polyclonal Chk-α antibody (dilution 1:100) (19), a mouse and human cross reactive rabbit polyclonal CHT1 antibody (dilution 1:2000) (Cat. No. NBP1-62339) Novus Biologicals, Littleton, CO), or a human and mouse cross reactive polyclonal CTL1 antibody (1:1000) (Cat. No. TA315247, OriGene). GAPDH (glyceraldehyde 3-phosphate dehydrogenase) was used as a loading control and detected with a human and mouse cross reactive monoclonal antibody (dilution 1:10000) (Cat. No. SAB1405848, Sigma). Immunoblots were developed using SuperSignal West Pico chemiluminescent substrate kit (Thermo Scientific, Rockford, IL). Because we used a human specific rabbit polyclonal Chk-α antibody we performed quantitative real-time polymerase chain reaction (q-RT-PCR) of normal mouse pancreas using primers designed for mouse *Chk*-α. Total RNA was isolated from tumor samples using the QIAshredder and RNeasy Mini kit (Qiagen, Valencia, CA). cDNA was prepared using the iScript cDNA synthesis kit (Bio-Rad, Hercules, CA). cDNA samples were diluted 1:10 and real-time PCR was performed using IQ SYBR Green supermix and gene specific primers in the iCycler real-time PCR detection system (CFX-96 Connect, Bio-Rad). All primers were designed using Beacon designer software 7.8

(PREMIER Biosoft, Palo Alto, CA). The expression of target RNA relative to the housekeeping ribosomal gene 18s (using corresponding mouse and human primers) was determined based on the threshold cycle (C_t) as $\Delta C_t = C_t$ of target gene - C_t of 18s. The 18s C_t values (Mean ± SEM) for normal mouse pancreas and for orthotopic tumors were 10.1 ± 0.06 (n = 3) and 9.9 ± 0.08 (n = 12) respectively.

Results

PDAC cell metabolism

Levels of Chk-α, CHT1, and CTL1 varied across the PDAC cell lines but were clearly higher than in non-neoplastic HPNE cells (Figure 1A). The HPNE cells showed no detectable levels of Chk-α expression and a low level of CHT1 and CTL1. Of the cancer cell lines, Pa04C and Pa28C had the lowest levels of Chk-α, while Pa03C had the lowest levels of both CHT1 and CTL1. Representative high-resolution ^{1}H MR spectra of the choline-containing metabolites region are shown in Figure 1B. Consistent with the non-detectable Chk-α expression and a low level of CHT1 and CTL1, the lowest levels of choline-containing metabolites were observed in the HPNE cells compared to the 8 PDAC cell lines investigated. Quantitative data for choline-containing metabolites obtained from water-soluble cell extracts are shown in Figure 1C. Significantly higher PC and tCho levels were observed in all the PDAC cell lines compared to the non-neoplastic HPNE cells. Amongst the cancer cells, Pa03C and Pa20C showed the highest PC levels. PC levels were the lowest in Pa04C and Pa28C cancer cells, consistent with the lowest Chk-α in these cells. There were no clear differences in the choline-containing compounds based on stage, or derivation from primary or metastatic cancers. Neither GPC nor Cho levels were consistently associated with PDAC.

Results from PCA are presented in Figure 2. The scattered PCA score plot (Figure 2A) shows a clustering of non-neoplastic HPNE pancreatic cells *versus* the pancreatic cancer cell lines. Multivariate PCA of the spectral data identified increases in lactate, acetate, glutamate, creatine, tCho, and myo-inositol, and decreases in alanine and aspartate in the cancer cells compared to the non-neoplastic cells (Figure 2B).

Tumor metabolism

Increases of PC and tCho observed in the cells were reflected in the ^{1}H MR spectra of subcutaneous tumor xenograft extracts (Figure 3A). Consistent with the cell data, additional metabolites such as alanine, creatine, phosphocreatine, lactate, and total creatine were observed in the tumor spectra. The patterns of these metabolites were different between the tumors. Harvested Panc1 tumors were characterized by the highest level of lactate, PC and tCho, Pa04C by the highest level of alanine, and BxPC3 and Panc1 had the highest level of creatine and total creatine (Figure 3B).

Altered choline metabolism in subcutaneous tumors

Immunoblot analysis revealed high Chk-α, CHT1 and CTL1 expression in all four xenografts (Figure 4A). Chk-α and CTL1 were highest in Panc1 tumors. As shown in Figure 4B, tCho was detected in all the subcutaneous tumor xenografts imaged *in vivo*. We

observed a heterogeneous distribution of the signal within each tumor and between each tumor type. Panc1 tumors presented with high tCho levels (Figure 4C), consistent with the tumor extract data, and with the high Chk-α and CTL1 expression observed in immunoblots obtained from these tumors.

Altered choline metabolism in orthotopic tumors

tCho was detected *in vivo* in orthotopically implanted tumors using 2D-CSI (Figure 5A) and single voxel ^{1}H MRS spectra (Figure 5B). We compared Chk-α, CHT1 and CTL1 in orthotopic tumors to protein lysate obtained from normal human pancreas. Similar to the subcutaneous tumors, increased Chk-α, CHT1 and CTL1 were observed in the orthotopic tumors compared to normal human pancreas. Also, similar to the observations made in subcutaneous tumors, Panc1 tumors presented with higher levels of Chk-α and CTL1 (Figure 5C). Normal mouse pancreas had undetectable levels of CHT1 and CTL1 (see Figure 4C). Unlike the CHT1 and CTL1 antibodies that are mouse and human cross-reactive, the Chk-α antibody was designed against human *Chk*-α. We therefore characterized Chk-α mRNA in mouse pancreas and in orthotopic human pancreatic cancer xenografts using primers for mouse and human Chk-α, respectively. We observed significantly higher Chk-α mRNA in the orthotopic tumors compared to normal mouse pancreas (Figure 5D).

Discussion

We observed a consistent increase of PC and tCho, and a consistently increased expression of Chk-α, CHT1 and CTL1 in a panel of human PDAC cell lines. The changes in choline metabolism and Chk-α, CHT1 and CTL1 were clearly due to malignant transformation since there was no dependence on whether these cancer cells originated from primary or metastatic tumors. These results identify PDAC as part of the increasing compendium of cancers that demonstrate altered choline metabolism following malignant transformation (7).

Orthotopic pancreatic cancer models have been previously developed (21) and represent an important advance in the investigation of this disease in compatible microenvironments, especially since expression of green or red fluorescent protein in these models provides the opportunity for noninvasive optical imaging of the tumors (22, 23). Although much of our metabolic characterization was performed with subcutaneous tumors, we also investigated choline metabolism in orthotopically implanted pancreatic tumors.

In tumors *in vivo*, the increased PC and tCho were primarily due to overexpression of Chk-α, as well as the choline transporters CHT1 and CTL1. Increased expression of CHT1 and CTL1 in other cancers has been previously reported (10, 13, 14). Other choline transporters and phospholipases (7) may also have contributed to the altered choline metabolism and should be further investigated. Chk-α, CHT1 and CTL1 may provide companion diagnostic molecular markers to detect pancreatic cancers. Patterns of choline metabolites, Chk-α, CHT1 and CTL1 observed in cultured cells were not entirely mirrored in the tumors *in vivo*. In culture, viable cells are maintained under carefully controlled conditions. *In vivo*, however, physiological conditions such as hypoxia, and the associated acidic extracellular pH that exist in pancreatic cancers (24), may affect choline phosphorylation and uptake

through effects on Chk-α (25) and transporters (13). Perfusion-limited delivery of substrates in poorly vascularized tumor regions will also influence metabolite concentrations *in vivo*. Additionally, necrosis and acute cell death, the extent of which varies between tumors, will also reduce levels of metabolites, enzymes, and transporters, contributing to differences between cells in culture and tumors *in vivo*. These factors can also explain variations in Chk-α, CHT1 and CTL1 expression within tumor groups, and between subcutaneous and orthotopic tumors. Despite some variations, the consistent pattern that emerged was an increase of tCho and Chk-α, CHT1 and CTL1 in PDAC cells and tumors.

The three noninvasive imaging methods currently used to detect PDAC are ultrasound (US), computed tomography (CT), and MRI. Endoscopic ultrasound is the primary method for imaging the pancreas and detecting small pre-invasive lesions. PDAC often presents as a mass with a loss of normal homogeneous parenchymal echo pattern (26). The sensitivity of US is ~ 95% if the lesion is more than 3 cm. With CT, which is the method of choice for evaluating patients with symptoms that are suggestive of the disease, lesions larger than 1.5 cm are detected at 100% but smaller lesions have a sensitivity of 77% and a specificity of 100% (27). The high soft tissue contrast of MRI provides an attractive option in staging PDAC (27). The desmoplastic stroma of PDAC prevents the delivery of contrast agents resulting in an absence of hyperintensity in the tumor compared to normal parenchyma that is useful in guiding resection and staging (27).

The pattern of increased choline transporters and Chk-α observed in several cancers has resulted in the development of radiolabeled choline analogs as positron emission tomography (PET) imaging tracers to detect cancers through the increased uptake and phosphorylation of the tracer (28, 29). Our data suggest that PET imaging of radiolabeled choline may be used to detect PDAC, provided there is adequate delivery of the probe, as the desmoplastic stroma in pancreatic cancers may impede its delivery (4). A recent study detected a relatively high uptake, but a low residence time, of a radiolabeled choline tracer in the pancreas of normal volunteers (30), suggesting that PDAC may be detected using relatively long-lived radiolabeled choline PET tracers that allow imaging at later time points to achieve good systemic clearance (30).

^{1}H MRSI has the advantage of detecting intrinsic metabolic contrast and does not require the delivery of an extrinsic marker for detection. Most clinical MRI scanners have the ability to perform proton MRS, making the incorporation of proton MRS with MRI easily achievable. Increased tCho, detected with ^{1}H MRS is consistently observed in cancer cells but not in nonmalignant cells (31–33). As a result, tCho detected by ^{1}H MRS is being evaluated as a diagnostic and prognostic biomarker in multiple human cancers (7). These human studies have confirmed that cancers have increased tCho (34, 35). Previous limitations due to motion artifact can now be minimized through motion-correction in acquisition and processing (36). Most diagnostic MRSI studies have focused on lesions with a size of 10 mm or greater (34), but the availability of higher field 3T magnets that are approved for clinical studies significantly increases the sensitivity of spectroscopic detection of tCho in cancers (37). Our results are also consistent with a previous study of tumors derived from Capan-1 human pancreatic cancer cells that showed increased signal intensity in the 3.2 ppm region of ^{1}H MR spectra, corresponding to the choline containing compound region (38).

These results support investigating the use of ^{1}H MRS as a diagnostic technique to complement existing technologies in detecting pancreatic cancer. Ultimately the ability of using ^{1}H MR spectroscopy to detect PDAC will depend upon tCho levels in normal pancreas. Recently, three human studies performed at 3T in a limited number of subjects have shown the feasibility of obtaining ^{1}H MR spectra from a voxel placed in the pancreas and in pancreatic cancers using breath-holding to minimize motion related artifacts (39–41). Although our orthotopic spectroscopic imaging data failed to detect tCho signal from normal pancreas, studies performed in humans suggest that the tCho signal may be relatively high in normal pancreas (41), depending upon whether the voxel is placed in the head or the body or tail of the pancreas (40). The head of the pancreas had significantly lower tCho normalized to water (40). In these studies, a lower tCho to water ratio was observed in the cancer voxels compared to normal pancreas (40, 41). Differences in water concentration between normal and fibrotic tissue, investigating large, potentially necrotic, lesions, and the less than optimum signal to noise levels were some of the limitations identified in these studies (40). Investigations comparing spectra obtained from normal and malignant pancreatic regions will require precise placement of voxels in viable non-necrotic tumor regions, elimination of motion-related effects, and accurate quantitation of metabolites. The use of MRSI that provides a tCho map rather than the placement of single voxels will address heterogeneities in the pancreas and in pancreatic cancers.

In addition to altered choline metabolism, differences in other metabolites were identified in PDAC cells compared to HPNE cells, some of which were also observed in the tumor extracts. PCA identified an increase in lactate, acetate, glutamate, creatine and myo-inositol and a decrease in alanine and aspartate in cancer cells compared to non-neoplastic pancreatic cells. Tumor extracts also showed differences in alanine, creatine, phosphocreatine and total creatine between the different tumor types. These results suggest that, in addition to enzymes in choline phospholipid metabolism, enzymes in glutaminolysis or glycolysis may provide new targets to treat PDAC. Studies have shown the efficacy of targeting Chk-α in preclinical studies of breast (19, 42), colon (43), bladder, lung and cervical cancers (44). A Chk-α inhibitor (TCD-717) is currently undergoing a Phase I clinical trial in cancer patients (NCT01215864). Decreased proliferation has been observed in pancreatic adenocarcinoma derived MIA PaCa-2 cells following glutamine deprivation (45).

In summary, our results have identified aberrant choline metabolism due to increased expression of Chk-α, CHT1, and CTL1 as well as differences in metabolites such as lactate and glutamate, in pancreatic cancer cells and tumors. These results create much-needed new possibilities for the detection of pancreatic cancer using ^{1}H MRS that merit rapid investigation in human subjects. Metabolic targets in choline phospholipid metabolism and in glutaminolysis and glycolysis may provide novel treatments for a disease that has severely limited treatment options.

Acknowledgement

This work was supported by NIH R01CA136576, R01CA138515, R01CA73850, R01CA82337, P50CA103175 and P30 CA006973. We thank Dr. V. P. Chacko for expert technical assistance.

Abbreviations

Chk	choline kinase
Cho	free choline
CHT1	high-affinity choline transporter
CTL1	choline transporter-like protein
CSI	chemical shift imaging
CT	computed tomography
GAPDH	glyceraldehyde 3-phosphate dehydrogenase
GPC	glycerophosphocholine
HPNE	human pancreatic nestin expressing
MRI	magnetic resonance imaging
MRS	magnetic resonance spectroscopy
MRSI	magnetic resonance spectroscopic imaging
PC	phosphocholine
PCA	principal component analysis
PDAC	pancreatic ductal adenocarcinoma
PET	positron emission tomography
q-RT-PCR	quantitative real-time polymerase chain reaction
tCho	total choline

References

1. Vincent A, Herman J, Schulick R, Hruban RH, Goggins M. Pancreatic cancer. Lancet. 2011; 378:607–620. [PubMed: 21620466]
2. Siegel R, Naishadham D, Jemal A. Cancer statistics, 2013. CA Cancer J Clin. 2013; 63:11–30. [PubMed: 23335087]
3. Ma J, Jemal A. The rise and fall of cancer mortality in the USA: why does pancreatic cancer not follow the trend? Future Oncol. 2013; 9:917–919. [PubMed: 23837751]
4. Whatcott, CJ.; Posner, RG.; Von Hoff, DD.; Han, H. Desmoplasia and chemoresistance in pancreatic cancer. In: Grippo, P.; Munshi, H., editors. Pancreatic Cancer and Tumor Microenvironemnt. 2012.
5. Steer ML, Waxman I, Freedman S. Chronic pancreatitis. N Engl J Med. 1995; 332:1482–1490. [PubMed: 7739686]
6. Kelly KA, Bardeesy N, Anbazhagan R, Gurumurthy S, Berger J, Alencar H, et al. Targeted nanoparticles for imaging incipient pancreatic ductal adenocarcinoma. PLoS Med. 2008; 5:e85. [PubMed: 18416599]
7. Glunde K, Bhujwalla ZM, Ronen SM. Choline metabolism in malignant transformation. Nat Rev Cancer. 2011; 11:835–848. [PubMed: 22089420]
8. Ramirez de Molina A, Rodriguez-Gonzalez A, Gutierrez R, Martinez-Pineiro L, Sanchez J, Bonilla F, et al. Overexpression of choline kinase is a frequent feature in human tumor-derived cell lines

and in lung, prostate, and colorectal human cancers. Biochem Biophys Res Commun. 2002; 296:580–583. [PubMed: 12176020]

9. Ramirez de Molina A, Banez-Coronel M, Gutierrez R, Rodriguez-Gonzalez A, Olmeda D, Megias D, et al. Choline kinase activation is a critical requirement for the proliferation of primary human mammary epithelial cells and breast tumor progression. Cancer research. 2004; 64:6732–6739. [PubMed: 15374991]
10. Eliyahu G, Kreizman T, Degani H. Phosphocholine as a biomarker of breast cancer: molecular and biochemical studies. Int J Cancer. 2007; 120:1721–1730. [PubMed: 17236204]
11. Ward CS, Eriksson P, Izquierdo-Garcia JL, Brandes AH, Ronen SM. HDAC inhibition induces increased choline uptake and elevated phosphocholine levels in MCF7 breast cancer cells. PLoS One. 2013; 8:e62610. [PubMed: 23626839]
12. Okuda T, Haga T, Kanai Y, Endou H, Ishihara T, Katsura I. Identification and characterization of the high-affinity choline transporter. Nat Neurosci. 2000; 3:120–125. [PubMed: 10649566]
13. Kouji H, Inazu M, Yamada T, Tajima H, Aoki T, Matsumiya T. Molecular and functional characterization of choline transporter in human colon carcinoma HT-29 cells. Archives of biochemistry and biophysics. 2009; 483:90–98. [PubMed: 19135976]
14. Inazu M, Yamada T, Kubota N, Yamanaka T. Functional expression of choline transporter-like protein 1 (CTL1) in small cell lung carcinoma cells: a target molecule for lung cancer therapy. Pharmacological research : the official journal of the Italian Pharmacological Society. 2013; 76:119–131. [PubMed: 23948665]
15. Jones S, Zhang X, Parsons DW, Lin JC, Leary RJ, Angenendt P, et al. Core signaling pathways in human pancreatic cancers revealed by global genomic analyses. Science. 2008; 321:1801–1806. [PubMed: 18772397]
16. Feldmann G, Dhara S, Fendrich V, Bedja D, Beaty R, Mullendore M, et al. Blockade of hedgehog signaling inhibits pancreatic cancer invasion and metastases: a new paradigm for combination therapy in solid cancers. Cancer Res. 2007; 67:2187–2196. [PubMed: 17332349]
17. Tkac I, Starcuk Z, Choi IY, Gruetter R. In vivo 1H NMR spectroscopy of rat brain at 1 ms echo time. Magn Reson Med. 1999; 41:649–656. [PubMed: 10332839]
18. Bolan PJ, Meisamy S, Baker EH, Lin J, Emory T, Nelson M, et al. In vivo quantification of choline compounds in the breast with 1H MR spectroscopy. Magn Reson Med. 2003; 50:1134–1143. [PubMed: 14648561]
19. Glunde K, Raman V, Mori N, Bhujwalla ZM. RNA interference-mediated choline kinase suppression in breast cancer cells induces differentiation and reduces proliferation. Cancer Res. 2005; 65:11034–11043. [PubMed: 16322253]
20. Savorani F, Tomasi G, Engelsen SB. icoshift: A versatile tool for the rapid alignment of 1D NMR spectra. J Magn Reson. 2010; 202:190–202. [PubMed: 20004603]
21. Fu X, Guadagni F, Hoffman RM. A metastatic nude-mouse model of human pancreatic cancer constructed orthotopically with histologically intact patient specimens. Proceedings of the National Academy of Sciences of the United States of America. 1992; 89:5645–5649. [PubMed: 1608975]
22. Bouvet M, Wang J, Nardin SR, Nassirpour R, Yang M, Baranov E, et al. Real-time optical imaging of primary tumor growth and multiple metastatic events in a pancreatic cancer orthotopic model. Cancer Res. 2002; 62:1534–1540. [PubMed: 11888932]
23. Katz MH, Takimoto S, Spivack D, Moossa AR, Hoffman RM, Bouvet M. A novel red fluorescent protein orthotopic pancreatic cancer model for the preclinical evaluation of chemotherapeutics. The Journal of surgical research. 2003; 113:151–160. [PubMed: 12943825]
24. Zhao X, Gao S, Ren H, Sun W, Zhang H, Sun J, et al. Hypoxia-inducible factor-1 promotes pancreatic ductal adenocarcinoma invasion and metastasis by activating transcription of the actin-bundling protein fascin. Cancer Res. 2014; 74:2455–2464. [PubMed: 24599125]
25. Glunde K, Shah T, Winnard PT Jr, Raman V, Takagi T, Vesuna F, et al. Hypoxia regulates choline kinase expression through hypoxia-inducible factor-1 alpha signaling in a human prostate cancer model. Cancer Res. 2008; 68:172–180. [PubMed: 18172309]
26. Niederau C, Grendell JH. Diagnosis of pancreatic carcinoma. Imaging techniques and tumor markers. Pancreas. 1992; 7:66–86.

27. Dabizzi E, Assef MS, Raimondo M. Diagnostic management of pancreatic cancer. Cancers (Basel). 2011; 3:494–509. [PubMed: 24212626]

28. DeGrado TR, Reiman RE, Price DT, Wang S, Coleman RE. Pharmacokinetics and radiation dosimetry of 18F-fluorocholine. Journal of nuclear medicine : official publication, Society of Nuclear Medicine. 2002; 43:92–96.

29. Witney TH, Alam IS, Turton DR, Smith G, Carroll L, Brickute D, et al. Evaluation of deuterated 18F- and 11C-labeled choline analogs for cancer detection by positron emission tomography. Clinical cancer research : an official journal of the American Association for Cancer Research. 2012; 18:1063–1072. [PubMed: 22235095]

30. Challapalli A, Sharma R, Hallett WA, Kozlowski K, Carroll L, Brickute D, et al. Biodistribution and radiation dosimetry of deuterium-substituted 18F-fluoromethyl-[1, 2-2H4]choline in healthy volunteers. Journal of nuclear medicine : official publication, Society of Nuclear Medicine. 2014; 55:256–263.

31. Aboagye EO, Bhujwalla ZM. Malignant transformation alters membrane choline phospholipid metabolism of human mammary epithelial cells. Cancer Res. 1999; 59:80–84. [PubMed: 9892190]

32. Ackerstaff E, Pflug BR, Nelson JB, Bhujwalla ZM. Detection of increased choline compounds with proton nuclear magnetic resonance spectroscopy subsequent to malignant transformation of human prostatic epithelial cells. Cancer Res. 2001; 61:3599–3603. [PubMed: 11325827]

33. Iorio E, Mezzanzanica D, Alberti P, Spadaro F, Ramoni C, D'Ascenzo S, et al. Alterations of choline phospholipid metabolism in ovarian tumor progression. Cancer Res. 2005; 65:9369–9376. [PubMed: 16230400]

34. Bolan PJ. Magnetic resonance spectroscopy of the breast: current status. Magn Reson Imaging Clin N Am. 2013; 21:625–639. [PubMed: 23928249]

35. Kurhanewicz J, Swanson MG, Nelson SJ, Vigneron DB. Combined magnetic resonance imaging and spectroscopic imaging approach to molecular imaging of prostate cancer. J Magn Reson Imaging. 2002; 16:451–463. [PubMed: 12353259]

36. Germuska M, Tunariu N, Leach MO, Xu J, Payne GS. An evaluation of motion compensation strategies and repeatability for abdominal (1)H MR spectroscopy measurements in volunteer studies and clinical trials. NMR in biomedicine. 2012; 25:859–865. [PubMed: 22190219]

37. Haddadin IS, McIntosh A, Meisamy S, Corum C, Styczynski Snyder AL, Powell NJ, et al. Metabolite quantification and high-field MRS in breast cancer. NMR Biomed. 2009; 22:65–76. [PubMed: 17957820]

38. Chemin-Thomas C, Esclassan J, Palevody C, Hollande E. Characterization of a specific signal from human pancreatic tumors heterotransplanted into nude mice. Study by high resolution 1H NMR and HPLC. Int J Pancreatol. 1993; 13:175–185. [PubMed: 8370979]

39. Su TH, Jin EH, Shen H, Zhang Y, He W. In vivo proton MRS of normal pancreas metabolites during breath-holding and free-breathing. Clinical radiology. 2012; 67:633–637. [PubMed: 22316597]

40. Ma X, Zhao X, Ouyang H, Sun F, Zhang H, Zhou C, et al. The metabolic features of normal pancreas and pancreatic adenocarcinoma: preliminary result of in vivo proton magnetic resonance spectroscopy at 3.0 T. Journal of computer assisted tomography. 2011; 35:539–543. [PubMed: 21926845]

41. Yao X, Zeng M, Wang H, Fei S, Rao S, Ji Y. Metabolite detection of pancreatic carcinoma by in vivo proton MR spectroscopy at 3T: initial results. La Radiologia medica. 2012; 117:780–788. [PubMed: 22095426]

42. Krishnamachary B, Glunde K, Wildes F, Mori N, Takagi T, Raman V, et al. Noninvasive detection of lentiviral-mediated choline kinase targeting in a human breast cancer xenograft. Cancer Res. 2009; 69:3464–3471. [PubMed: 19336572]

43. de la Cueva A, Ramirez de Molina A, Alvarez-Ayerza N, Ramos MA, Cebrian A, Del Pulgar TG, et al. Combined 5-FU and ChoKalpha inhibitors as a new alternative therapy of colorectal cancer: evidence in human tumor-derived cell lines and mouse xenografts. PLoS One. 2013; 8:e64961. [PubMed: 23762272]

44. Banez-Coronel M, Ramirez de Molina A, Rodriguez-Gonzalez A, Sarmentero J, Ramos MA, Garcia-Cabezas MA, et al. Choline kinase alpha depletion selectively kills tumoral cells. Curr Cancer Drug Targets. 2008; 8:709–719. [PubMed: 19075594]

45. Commisso C, Davidson SM, Soydaner-Azeloglu RG, Parker SJ, Kamphorst JJ, Hackett S, et al. Macropinocytosis of protein is an amino acid supply route in Ras-transformed cells. Nature. 2013; 497:633–637. [PubMed: 23665962]

Statement of translational relevance

Pancreatic ductal adenocarcinoma (PDAC) is an aggressive and lethal disease that develops relatively symptom-free and is therefore advanced at the time of diagnosis. The poor prognosis of PDAC is due to a combination of late-stage diagnosis and limited response to chemotherapy and radiotherapy, arising in part from the strong desmoplastic stroma that limits delivery of diagnostic imaging probes and therapeutic agents. The absence of early symptoms and effective treatments has created a critical need for identifying and developing new noninvasive biomarkers and therapeutic targets.

Our results have identified aberrant choline metabolism as well as differences in lactate and glutamate in human pancreatic cancer cells and xenografts. These results create much-needed new possibilities to detect pancreatic cancer using ^{1}H MRS that merit rapid investigation in human subjects. Metabolic targets in choline phospholipid metabolism and in glutaminolysis and glycolysis may provide novel treatments for a disease that has severely limited treatment options.

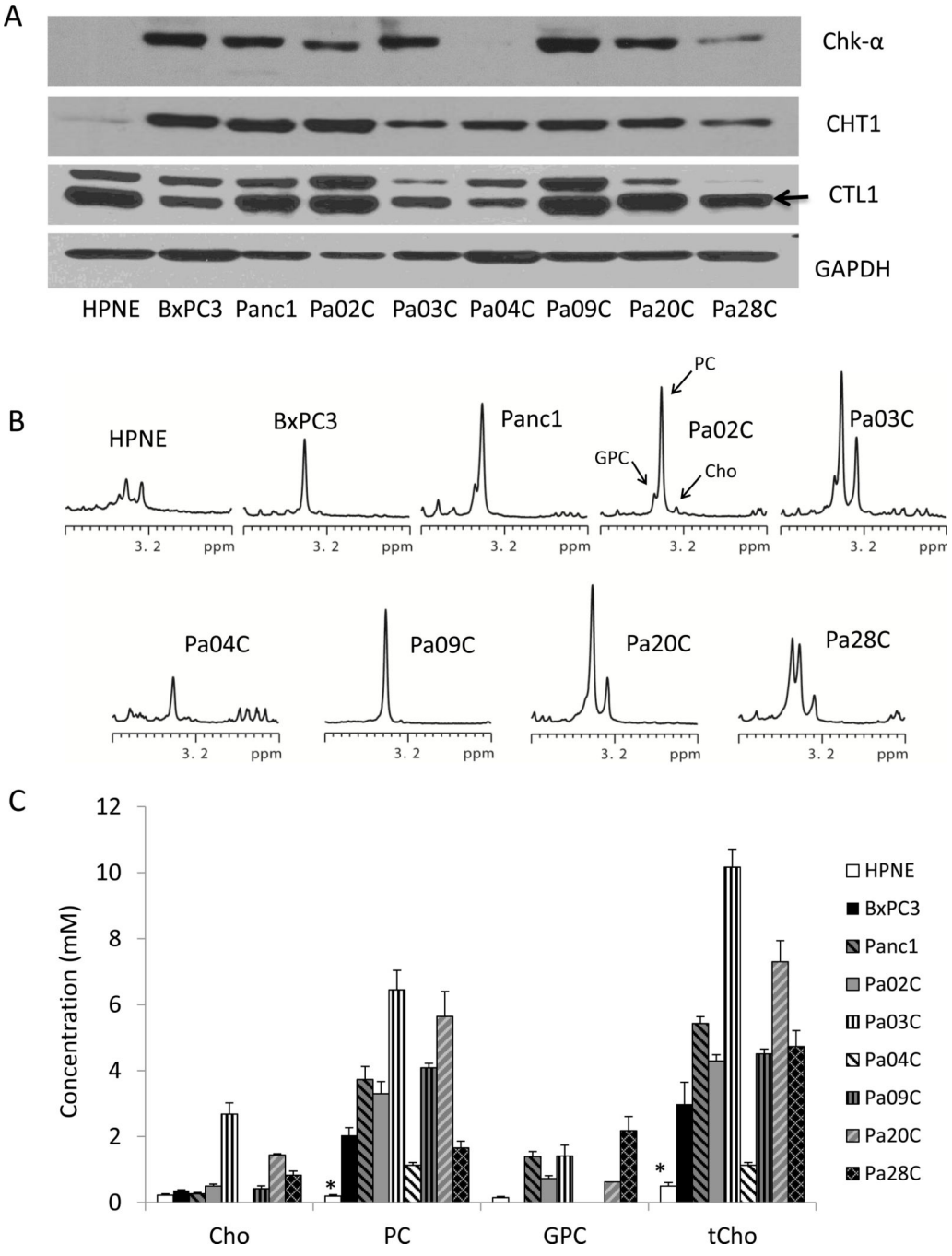

Figure 1.

(A) Representative immunoblots from a panel of pancreatic cell lines showing Chk-α, CHT1, and CTL1 expression with GAPDH as loading control. (B) Representative high-resolution ^{1}H spectra of the choline-containing compounds region obtained from HPNE and PDAC cell lines. (C) Quantitative data for choline-containing compounds in a panel of pancreatic cell lines. Cho: free choline, PC: phosphocholine, GPC: glycerophosphocholine, tCho: total choline. Values represent Mean ± SEM, n = 4. * $P < 0.05$ HPNE *vs* all.

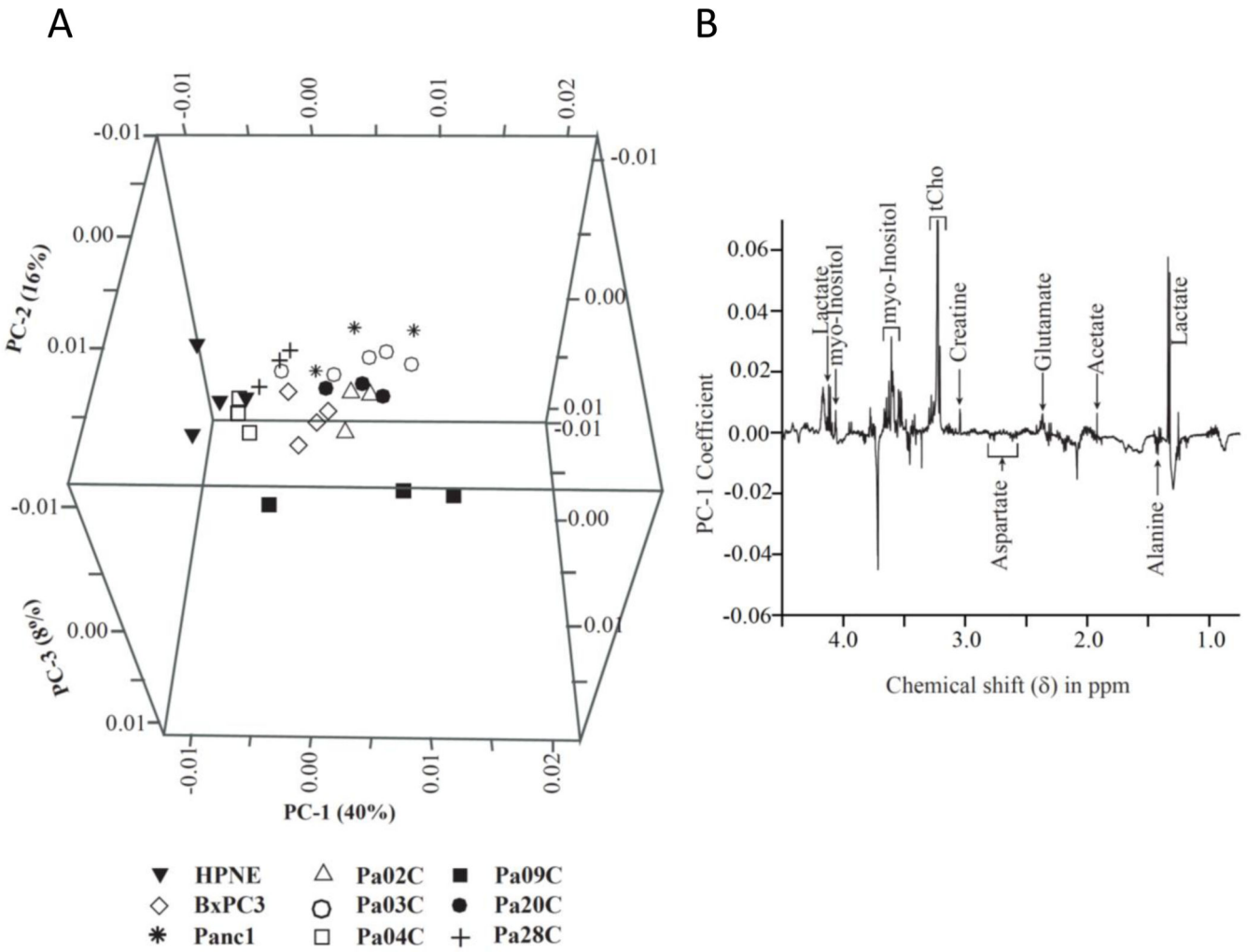

Figure 2.

(A) PCA of the high-resolution spectral data-derived score plots of water-soluble cell extracts, showing clustering differences between non-malignant HPNE *vs* PDAC cell lines based on differences in their overall metabolic profile. (B) PCA analysis shows increased lactate, tCho, acetate, glutamate, creatine, myo-inositol, and decreased alanine and aspartate in PDAC cells compared to non-malignant HPNE cells.

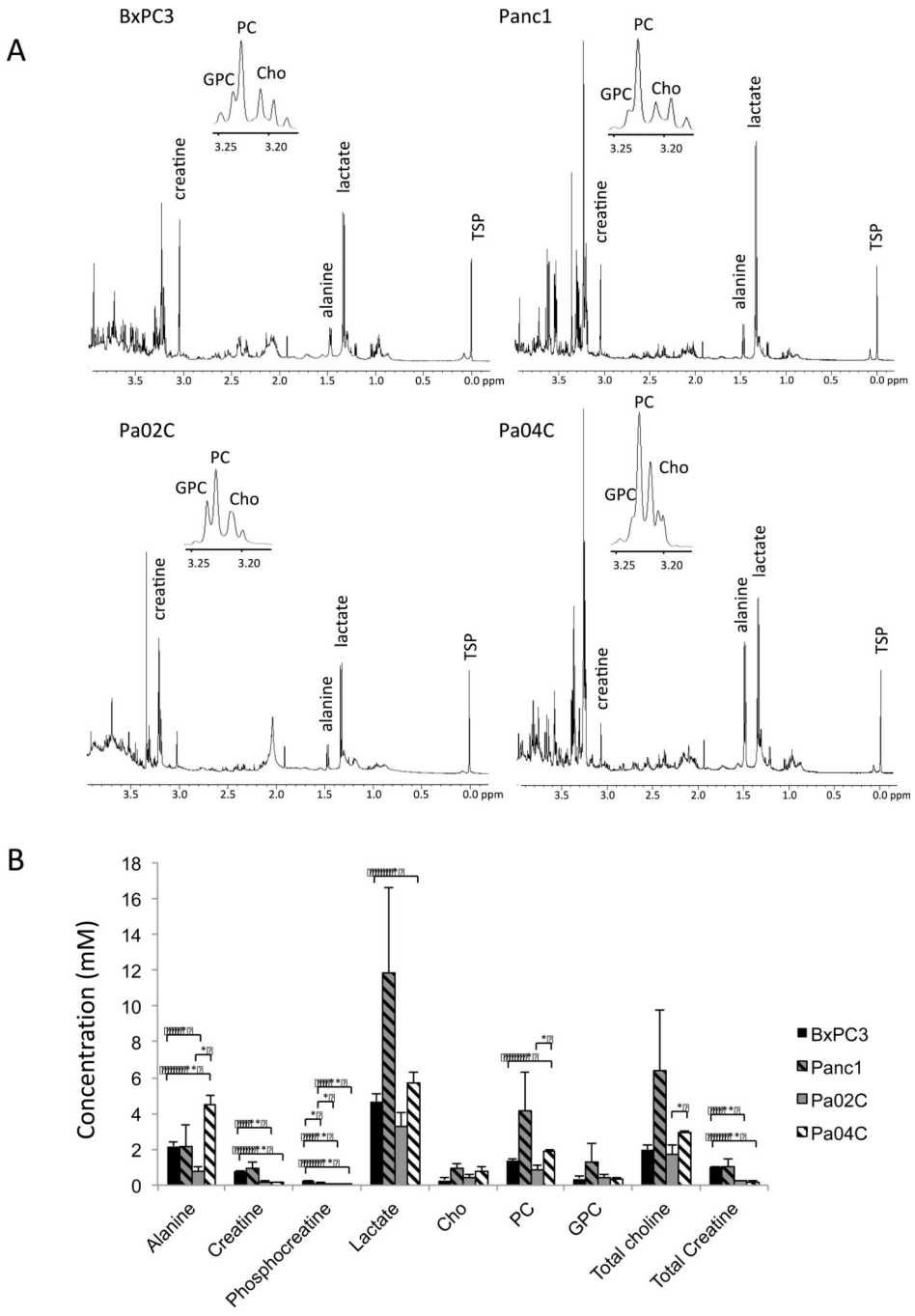

Figure 3.

(A) Representative ^{1}H MR high-resolution spectra of water-soluble BxPC3, Panc1, Pa02C, and Pa04C tumor extracts. (B) Concentration of water-soluble metabolites in BxPC3, Panc1, Pa02C, and Pa04C tumors (n = 3 per group, * $P < 0.05$, ** $P < 0.001$). Values represent Mean ± SEM. Cho: free choline, PC: phosphocholine, GPC: glycerophosphocholine, tCho: total choline.

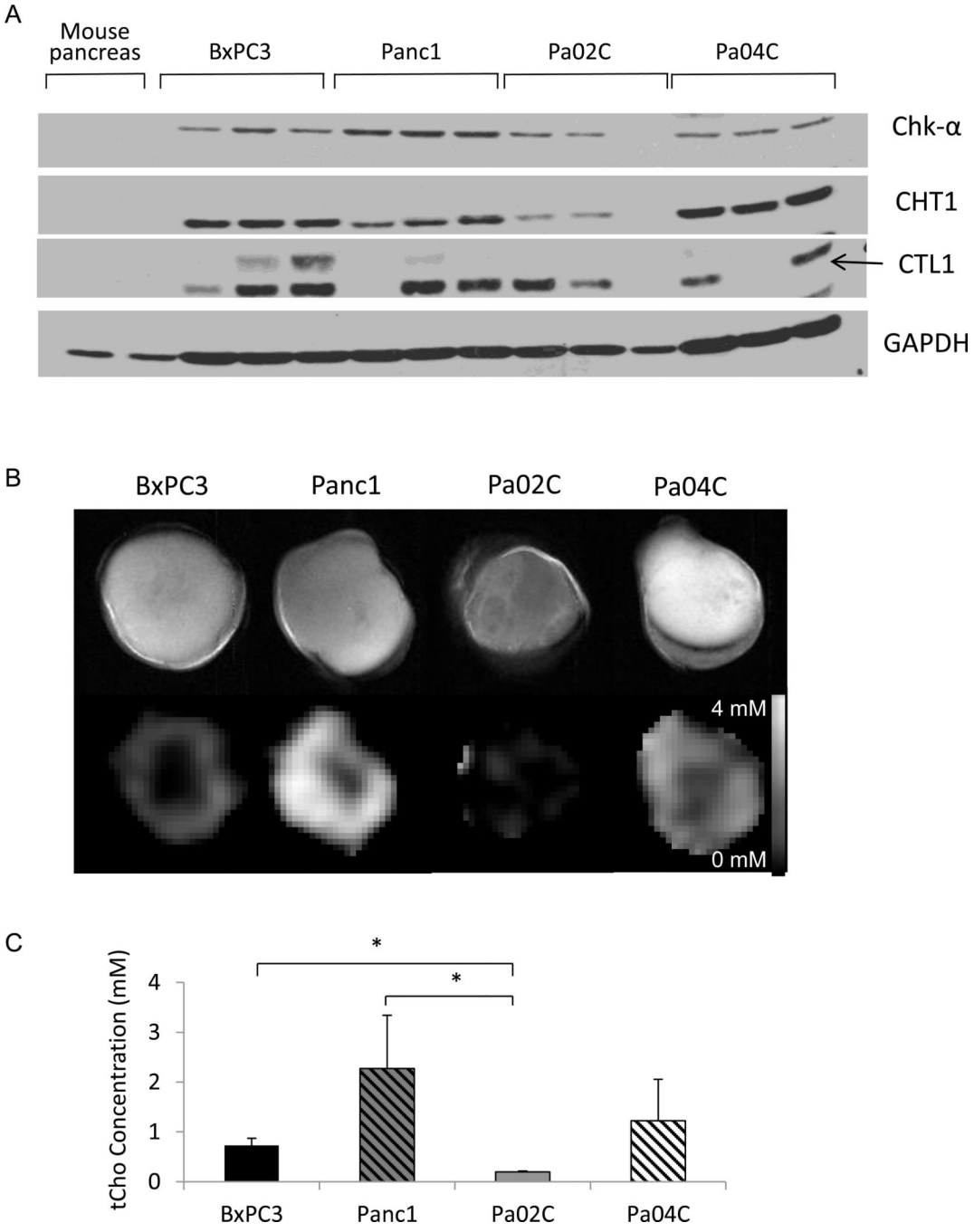

Figure 4.

(A) Representative immunoblots showing Chk-α, CHT1, and CTL1 proteins in BxPC3, Panc1, Pa02C, and Pa04C tumors, and in tissue obtained from normal mouse pancreas. GAPDH was used as loading control (n = 3). The arrow marks CTL1. (B) Representative anatomical images of BxPC3, Panc1, Pa02C, and Pa04C tumors (top row), and corresponding representative tCho maps (bottom row). (C) tCho concentrations in Pa04C, BxPC3, Pa02C and Panc1 tumors (n = 3 per group, * $P < 0.05$).

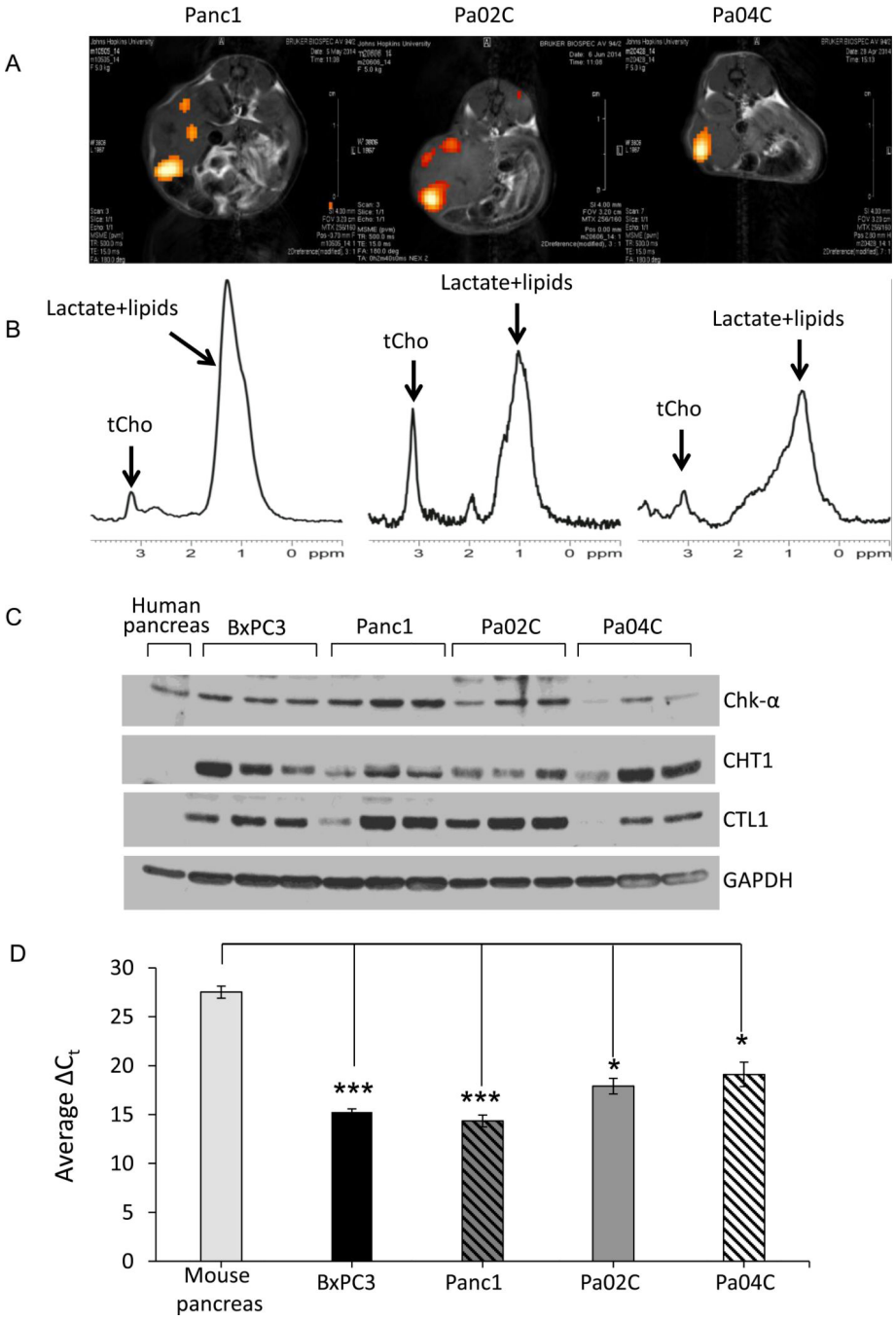

Figure 5.

(A) Images of tCho overlaid on anatomic images from mice bearing orthotopic Panc1, Pa02C, and Pa04C tumors. (B) Corresponding single voxel (5 mm^3) spectra localized in the center of the tumor. (C) Representative immunoblots showing Chk-α, CHT1 and CTL1 proteins in normal human pancreas and in orthotopic BxPC3, Panc1, Pa02C, and Pa04C tumors. GAPDH was used as loading control. (D) Differences in Chk-α mRNA in normal mouse pancreas, and in orthotopic BxPC3, Panc1, Pa02C, and Pa04C tumors, using 18s

ribosomal RNA as a reference gene. $\Delta C_t = C_t$ of Chk-α − C_t of 18s. Values represent Mean ± SEM, n = 3 per group, *** $P < 0.0005$, * $P < 0.05$.

Table 1

Details of pancreatic cell lines studied.

Cell line	Source	Tissue derivation	Carcinoma type	Stage	Sex
HPNE	ATCC	Non-neoplastic human pancreatic duct	-	-	M
BxPC3	ATCC CRL1687	Primary pancreatic tumor	Ductal adenocarcinoma	-	F
Panc1	ATCC CRL1469	Primary pancreatic tumor	Ductal adenocarcinoma	-	M
Pa02C	JHU	Liver metastasis	Ductal adenocarcinoma	IV	M
Pa03C	JHU	Liver metastasis	Ductal adenocarcinoma	IV	M
Pa04C	JHU	Lung metastasis	Ductal adenocarcinoma	IV	M
Pa09C	JHU	Primary pancreatic tumor	Ductal adenocarcinoma	IIb	F
Pa20C	JHU	Primary pancreatic tumor	Ductal adenocarcinoma	IIb	M
Pa28C	JHU	Primary pancreatic tumor	Ductal adenocarcinoma	IIb	M